Desalination and Water Treatment
www.deswater.com

doi: 10.1080/19443994.2013.846240

53 (2015) 826–835
January

Taylor & Francis
Taylor & Francis Group

Kinetics, thermodynamics, and isotherm studies for the adsorption of BR2 dye onto avocado integument

Farzaneh Marahel[a], Moonis Ali Khan[b,*], Ehsan Marahel[a,c], Iman Bayesti[a,c], Soraya Hosseini[a,c]

[a]*Chemistry Department, Islamic Azad University, Omidiyeh Branch, Omidiyeh, Iran*
[b]*Advance Material Research Chair, Chemistry Department, College of Science, King Saud University, Riyadh 11451, Saudi Arabia*
Emails: mokhan@ksu.edu.sa; moonisalikhan@gmail.com
[c]*Department Chemical and Environmental Engineering, Universiti Putra Malaysia, 43400 UPM, Serdang, Selangor, Malaysia*

Received 17 July 2013; Accepted 3 September 2013

ABSTRACT

Ability of avocado integuments (AI), an agricultural waste, to adsorb Basic Red 2 (BR2) was studied by batch process. Effect of parameters such as initial adsorbate solution pH, adsorbent dosage, initial adsorbate concentration, contact time, temperature, and background electrolyte on BR2 adsorption was studied. The BR2 adsorption was optimum (15.6 mg/g) at pH: 7. Acid-base titration studies showed dominance of acidic sites on AI surface. Two and three parameter isotherm models such as Langmuir, Freundlich, Toth, Redlich–Peterson, and Sips were applied to isotherm data. Studies showed Sips model applicability as revealed by linear, nonlinear isotherms, and statistical error functions. Contact times studies showed that 70% of BR2 adsorption at various concentrations on AI was achieved in 180 min. Pseudo-first-order, pseudo-second-order, and intra-particle diffusion models were applied to kinetics data. Results revealed applicability of pseudo-second-order kinetics model. Intra-particle diffusion plots at various BR2 concentrations were nonlinear over the entire contact time range indicating involvement of two or three steps during adsorption. Thermodynamic studies revealed endothermic and spontaneous process.

Keywords: Basic Red 2; Avocado integument; Physisorption; Sips model; Endothermic

1. Introduction

Industries such as textile, paper and pulp, rubber, cosmetic, pharmaceutical, and food are well known for the usage of synthetic dyes. Ease to use and low cost are some of the merits of using synthetic alternatives compared to natural dyes [1]. However, the discharge of dyes containing industrial effluents adds undesirable color to water bodies, preventing the penetration of sunlight, retarding photosynthetic reactions [2], and affecting aquatic life. Skin irritation, cancer, dermatitis, and mutation in human beings are the other demerits of synthetic dyes [3]. Considering the hazardous effects of dyes development of efficient remediation techniques is of paramount interest.

Various treatment techniques such as conventional physicochemical and biological treatment, chemical

*Corresponding author.

coagulation/flocculation, ozonation, oxidation, and adsorption have been utilized for the abatement of dyes. Adsorption has proved to be the most effective technique among them. Low operational cost, ease of operation, and removal of dyes from aqueous phase even at trace levels are some of the merits of adsorption process. Moreover, adsorption has also been widely used for the removal of certain class of chemical pollutants from water especially those that are non-biodegradable [4]. Various synthetic and physico-chemically modified adsorbents such as carbon coated monolith [5], surfactant-modified natural zeolite [6], and hypercross-linked polymeric adsorbent [7] have been reported for the removal of dyes. To make adsorption economically and ecologically feasible process, research is going on to explore better alternatives (adsorbents). Presently, researchers are focusing on utilization of industrial and agricultural wastes as adsorbents as it could be a better waste management alternative [8,9]. De-oiled soya waste, hen feather, wheat husk, coconut husk, and bottom ash were utilized for the removal of eosin yellow, congo red, amaranth, amido black 10B, brilliant yellow, yellow ME 7 G, quinoline yellow, and acid red 27, respectively [10–17].

Avacado (*Persea Americana*), a native tree of Central Mexico, belongs to *Lauraceae* family of kingdom Plantae along with cinnamon and camphor [18]. Previous studies reported utilization of avacado kernel seeds activated carbon for phenol removal with 90 mg/g maximum monolayer adsorption capacity at 298 K [19]. Devi [20] studied chemical oxygen demand and biological oxygen demand removal from coffee wastewater by avocado seed carbon with maximum reduction 98.28 and 99.19%, respectively. The removal of hexavalent and total chromium by avocado shell was studied with 101.81 and 61.67 mg/g removal capacity, respectively [21]. To our knowledge, none of the studies have reported utility of Avocado integuments (AI) for BR2 dye removal. Basic Red 2 ($C_{20}H_{19}ClN_4$) synonymously known as Safranin is commonly used for colorings and as a redox indicator. The objective of this research was to investigate the feasibility of AI as adsorbent for the removal of BR2. The influence of various parameters such as initial adsorbate solution pH, concentration, temperature, adsorbent dose, contact time, and ionic salt was tested.

2. Experimental

2.1. Preparation of adsorbent

AI were collected form a local oil factory. They were washed with deionized (D.I) water to remove dust and were dried in an open air oven at 80°C for 48 h. Dried biomass was then grounded to a desired particle size (100–120 μm). The crushed biomass was then treated with (H_2O_2; 30% w/w) to oxidize organic matter present. The oxidized biomass was further washed with D.I water until it attains neutral pH value. Finally, the biomass was dried overnight at 80° C. In order to prevent biomass from moisture and dirt, it was stored in sealed plastic bags and was kept in a desiccator.

2.2. Characterization of AI

Fourier transform infrared (FT-IR, Perkin–Elmer Norwalk) analysis was performed in range 4,000–400 cm^{-1} to identify the functional groups present on AI surface. Boehm's acid-base titration study [16] was performed to determine the concentration of acid and base functionalities on the surface of AI. To a series of 50-mL conical flasks containing 0.1 N NaOH, 0.1 N $NaHCO_3$, 0.1 N Na_2CO_3, and 0.1 N HCl solutions, 0.5 g AI (each) was added. The flasks were then sealed and were kept on manual shaking for five days. Afterward, the alkaline solutions (0.1 N NaOH, 0.1 N $NaHCO_3$, and 0.1 N Na_2CO_3) were titrated with 0.1 N HCl solution while, the acid solution (0.1 N HCl) was titrated with 0.1 N NaOH. Finally, the concentration of acidic and basic sites was calculated. Solid addition method was used to determine surface charge of AI. Series of conical flasks (250 mL) containing 0.01 N KNO_3 solution were taken. The initial pH (pH_i) of solution in each flask was adjusted between 2 and 10 by adding 0.1 N KOH or 0.1 N HNO_3. The flasks were manually agitated and were kept for 24 h under ambient temperature conditions. After 24 h, samples were filtered, and final pH (pH_f) was measured. The difference between pH_i and pH_f was plotted versus pH_i to obtain point of zero charge (pH_{PZC}) value of AI [22].

2.3. Adsorption studies

Batch mode adsorption studies were carried out. Adsorbate solution (250 mL) of desired initial concentrations (C_o—25–150 mg/L) was taken in conical flasks (250 mL) and was equilibrated with 0.8 g of adsorbent on a shaker at 150 rpm under ambient temperature conditions. At equilibrium, supernatant was centrifuged and equilibrium concentration (C_e) of BR2 was measured by visible spectrophotometer (ET99731 Tintometer GmbH, Germany) at maximum wavelength (λ_{max})—530 nm [23,24]. The adsorption capacity at equilibrium (q_e, mg/g) was then calculated by mass balance equation given as:

$$q_e = (C_o - C_e) \times \frac{V}{m} \quad (1)$$

where C_o and C_e (mg/L) are the initial and equilibrium concentrations of dye, respectively, V is the volume of the adsorbate solution (L) and m is the mass of adsorbent (g).

Thermodynamics studies were conducted for a concentration range 25–150 mg/L by varying reaction temperature from 30 to 50°C. While pH studies were conducted in pH range: 2–10. The contact time studies were also conducted for a concentration range 25–150 mg/L, samples were collected at specified time intervals until equilibrium was achieved. The adsorption capacity at equilibration time t (q_t, mg/g) was then calculated by mass balance equation given as:

$$q_t = (C_o - C_t) \times \frac{V}{m} \quad (2)$$

where C_t (mg/L) is equilibrium concentration at time t.

3. Results and discussion

3.1. Characterization of adsorbent

The surface functionalities as determined by acid-base titrations showed dominance of acidic sites (carboxylic—0.378 mmol/g, lactonic—0.001 mmol/g, and phenolic—0.411 mmol/g) compared to basic sites (0.012 mmol/g). Infrared spectroscopic study was carried out to find the functional groups present on AI surface and involved in BR2 binding over AI. Fig. 1 shows the FT-IR spectra of AI before and after BR2 adsorption. A broad, intense absorption peak around 3,350 cm^{-1} indicative of the existence of bounded hydroxyl groups. A peak observed at 2,924 cm^{-1} indicative of asymmetric and symmetric stretching C–H group vibrations. A weak intensity bands ascribed to C≡C bond appeared between 2,200 and 2,300 cm^{-1}. Two overlapped bands around 1,730 cm^{-1} and 1,600 cm^{-1} in spectra were assigned to C=O stretch vibrations. A strong absorption C–O stretch band appears in region at 1,030–1,250 cm^{-1}. The FT-IR spectrum after BR2 adsorption showed weakening or disappearance of peaks at 3,350, 2,924, and 1,030 cm^{-1} confirming active involvement of these surface groups in BR2 adsorption of AI. This also showed an
electrostatic interaction between cationic BR2 dye and surface active groups on AI.

3.2. Effect of pH

Solution pH plays a major role controlling in adsorption process by affecting protonation of surface groups, degree of ionization of dye, and solution composition. Therefore, pH parameter study is of value. In present work, the effect of pH was studied in pH range: 2–10. Reported pKa of BR2 was 6.4 [25]. As revealed by FT-IR studies, hydroxyl (–OH) and carboxyl (–COOH) were the active functional groups. Both groups were protonated at lower pH while deprotonated to $–OH^-$, $–COO^-$ at higher pH. Cationic

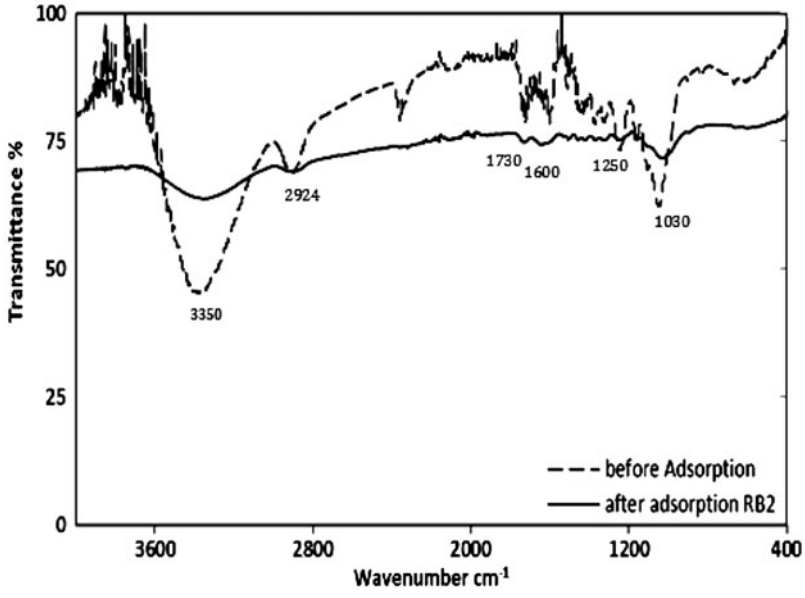

Fig. 1. FT-IR spectra of AI.

dye adsorption favored at pH > pKa due to the presence of functional groups such as OH^-, COO^- groups. Fig. 2a shows the uptake of BR2 on AI at various pH values. At lower pH, nitrogen atom was found to be in protonated form and the active sites on adsorbent surface were less available for cationic dye due to greater repulsive force which further leads to a decrease in dye uptake. Considerable increase in BR2 adsorption on AI was observed in pH range: 2–5 attaining optimum adsorption (15.6 mg/g) at pH: 7. Increase in pH above 7 leads to decrease in adsorption. Also, as demonstrated in Fig. 2b, the observed pH_{pzc} of adsorbent was 6.5. The decrease in adsorption above pH_{PZC} might be due to the dissociation of acidic surface functionalities with increase in pH giving rise to negative charge on the dye molecule [26].

3.3. Effect of adsorbent dosage

The effect of AI dosage on BR2 adsorption was observed by varying AI dose from 0.1 to 0.9 g. A series of conical flasks containing 250 mL adsorbate solution (C_o—60 mg/L) were taken. The adsorbate solutions were equilibrated at 30˚C for 3 h on a mechanical stirrer at 150 rpm. The % adsorption increased from 31.4 to 95.4% with increase in adsorbent dose from 0.1 to 0.9 g (Fig. 3), respectively. The BR2 adsorption increased from 31.43 to 88% with increase in AI dose from 0.1 to 0.5 g, respectively. Further, increase in dose form 0.6 to 0.9 g showed no appreciable increase in adsorption. The increase in adsorption may be attributed to increased AI surface area and availability of more adsorption sites for BR2 adsorption. However, the adsorption capacity decreased from 44.22 to 14.83 mg/g for aforementioned AI dose. The decrease in adsorption capacity might be due to overlapping or aggregation of adsorption sites available for BR2 adsorption over AI surface and increase in diffusion path length [27].

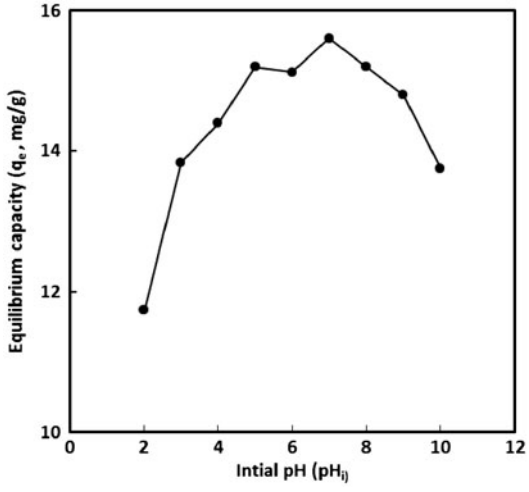

Fig. 2a. Effect of pH on BR2 adsorption on AI.

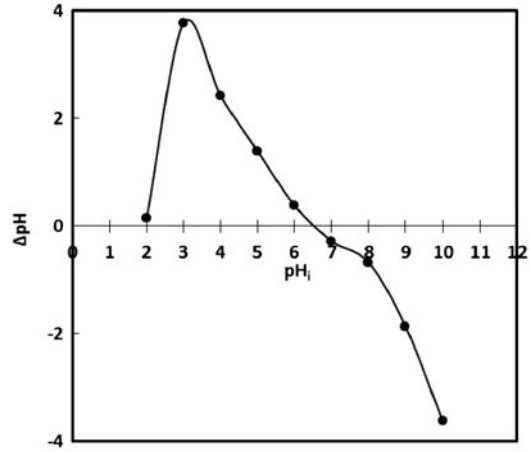

Fig. 2b. pHPZC of AI using 0.1 M KNO3.

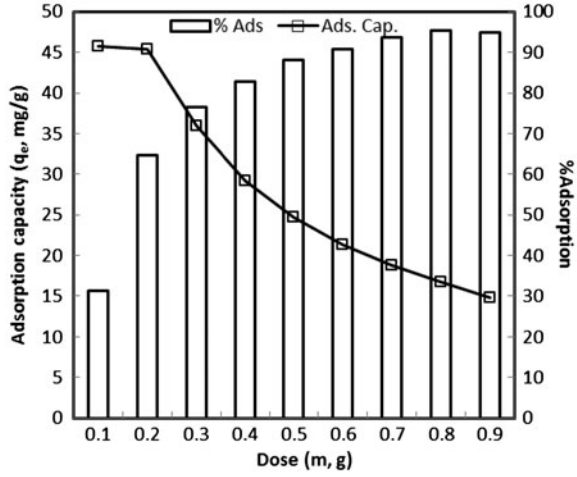

Fig. 3. Effect of dose on BR2 adsorption on AI.

3.4. Effect of contact time

The contact time studies were carried out at various BR2 concentrations (C_o—25–150 mg/L) under ambient temperature (30˚C) conditions. The adsorbate solution (pH_i: 7) was treated with 0.8 g of AI in a conical flask (250 mL) on a mechanical stirrer with agitation speed 150 rpm. The samples were collected at specified time. Initially, the adsorption of BR2 on AI at various concentrations was fast, gradually slows down with time, finally attaining equilibrium (Fig. 4). The observed BR2 adsorption at various concentrations on AI for initial 180 min contact time was 70%. This might be due to abundantly available active sites

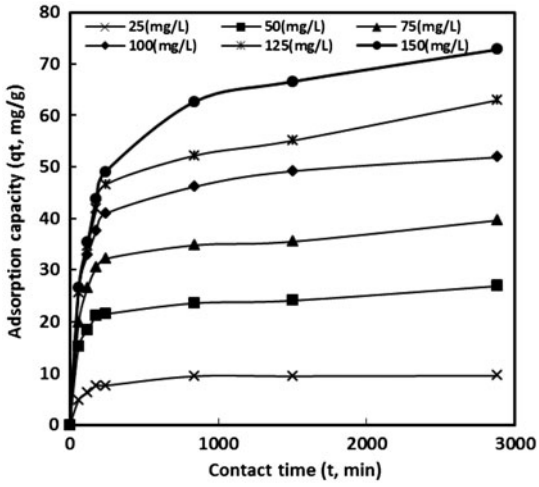

Fig. 4. Effect of contact time on BR2 adsorption at various concentrations on AI.

on adsorbent surface [28,29]. As time lapse, the active sites on adsorbent surface gradually decreased lowering BR2 uptake, finally attaining equilibrium. Equilibrium reached is not only due to the saturation of active sites of AI surface but may also be due to the reduction in the adsorbate concentration gradient. The equilibrium capacity increased from 9.54 to 72.74 mg/g with increase in BR2 concentration from 25 to 150 mg/L, respectively, with equilibration time varies between 840 and 1,500 min. The higher adsorbate concentration enhances the driving force for the adsorption process. Therefore, increase in equilibrium capacity was observed with increase in initial BR2 concentration.

3.5. Adsorption isotherm studies

Adsorption isotherm studies are essential to describe interaction between adsorbent and adsorbate at equilibrium condition. In present study, two and three parameter isotherm models were applied (Table 1) as in some cases two parameter models are not competent enough; therefore, a suitable curve fitting may be provided by three parameter models. To check out best fitted model to experimental data, different error functions were also examined (Table 2) [30]. The best fit model was evaluated by highest correlation coefficient (r^2) [31] and lowest error function values.

The two parameter models such as Langmuir and Freundlich and three parameter models such as Redlich–Peterson, Toth, and Sips models were applied to experimental data in both linear and nonlinear isotherm forms. The optimization of nonlinear isotherm requires an error function to be used in order to evaluate the fitting of the isotherm models on the experimental data. The best fit model was evaluated in terms of r^2, standard error function (SSE), average relative error (ARE), residual sum of squares (RSS), and mean relative error (MRE).

Results suggest that Sips model yielded the highest r^2 (linear and nonlinear) and lowest SEE value (Tables 3 and 4). For both linear and nonlinear isotherms, Langmuir model showed more difference with the equilibrium data with lowest r^2 values (Table 3). Fig. 5 shows Sips, Freundlich, Toth, and Redlich–Peterson were superposed to experimental data while Langmuir showed slight scattering from the experimental data. The sum of the normalized

Table 2
Statistical error functions

Error function	Equation
Standard error estimate	$\mathrm{SEE} = \sqrt{\frac{\sum (q_{\mathrm{exp}} - q_{\mathrm{cal}})^2}{N}}$
Average relative error	$\mathrm{ARE} = \frac{100}{N}\sum_{i=1}^{N}\left\lvert\frac{(q_{\mathrm{exp}} - q_{\mathrm{cal}})}{q_{\mathrm{exp}}}\right\rvert$
Mean relative error	$\mathrm{MRE} = \frac{1}{N}\sum_{i=1}^{N}(q_{\mathrm{cal}} - q_{\mathrm{exp}})^2$
Residual sum squares	$\mathrm{RSS} = \sum (q_{\mathrm{exp}} - q_{\mathrm{cal}})^2$

Table 1
Adsorption isotherm models

Isotherm	Expressions		Parameters
	Non-linear	Linear	
Langmuir	$q_e = \frac{q_m k_L C_e}{1 + k_L C_e}$	$\frac{C_e}{q_e} = \frac{1}{k_L q_m} + \frac{1}{q_m} \times C_e$	q_m (mg/g), k_L (L/mg)
Freundlich	$q_e = k_F C_e^{1/n}$	$\log q_e = \log k_F + \frac{1}{n}\log C_e$	k_F (mg/g) (L/mg)$^{1/n}$, n
Toth	$q_e = \frac{k_T C_e}{(a_T + C_e)^{1/\tau}}$	$\ln\left(\frac{q_e}{k_T}\right) = \ln(C_e) + \frac{1}{\tau}\ln(a_T + C_e)$	a_T (mg/g), k_T (L/mg), τ
Sips	$q_e = \frac{q_m k_s C_e^{\lambda}}{1 + k_s C_e^{\lambda}}$	$\lambda \mathrm{Ln}(C_e) = -\mathrm{Ln}(\frac{q_m k_s^{\lambda}}{q_e}) + \lambda \mathrm{Ln}(k_s)$	q_m (mg/g), k_s (L/g), λ
Redlich–Peterson	$q_e = \frac{q_{PR} k_{RP} C_e}{1 + k_{RP} C_e^{\gamma}}$	$\mathrm{Ln}(K_R \frac{C_e}{q_e} - 1) = \mathrm{Ln}a_R + \beta \mathrm{Ln}C_e$	q_{PR} (mg/g), k_{RP} (L/g), γ

Table 3
Isotherm parameters for the adsorption of BR2 on AI

Isotherm	Parameters	Values	
		Non-linear	Linear
Redlich–Peterson	q_{PR} (mg/g)	11.02	17.04
	k_{RP} (L/g)	40284.8	18
	γ	0.486	0.5723
	r^2	0.9884	0.9590
Freundlich	k_f (mg/g) (L/mg)$^{1/n}$	10.79	9.526
	$1/n$	0.521	0.564
	r^2	0.9885	0.9270
Langmuir	q_m (mg/g)	102.45	91.74
	k_L (L/mg)	0.056	0.077
	r^2	0.9713	0.9580
Toth	a_T (mg/g)	0.737	5
	k_T (L/mg)	12.537	2
	$1/\tau$	0.520	0.5723
	r^2	0.9898	0.9590
Sips	q_m (mg/g)	1023.237	75
	k_s (L/g)	0.001	0.1023
	λ	0.537	0.564
	r^2	0.9895	0.9790

Table 4
Error functions for different adsorption isotherm models

Isotherm	Error functions				
	SSE	ARE	RSS	MRE	ΣSNE
Redlich–Peterson	3.234	7.007	31.375	4.934	1.484
Freundlich	2.816	7.744	31.375	5.229	1.503
Langmuir	4.852	7.053	91.957	15.326	1.296
Toth	3.077	6.996	28.127	4.688	1.525
Sips	0.206	6.772	31.219	5.203	1.390

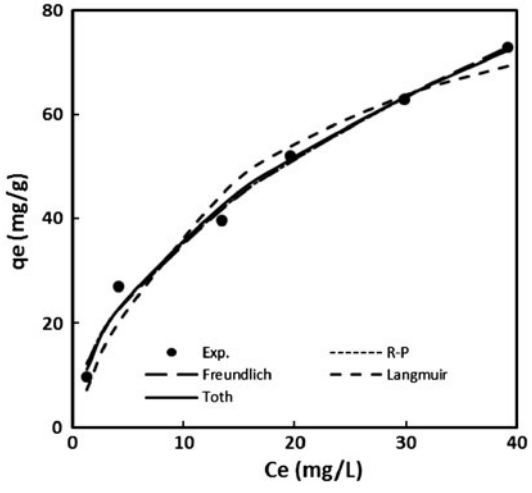

Fig. 5. Nonlinear isotherm plot for BR2 adsorption on AI.

errors values (ΣSNE) was used in order to determine the optimum isotherm parameters. This parameter was a summation of total errors produced. It can be obtained by dividing the error values with the maximum error value [31,32]. Hence, it could be concluded that Sips model was best applicable model. Sips model is a conjugation of Langmuir and Freundlich expressions deduced for predicting the heterogeneous adsorption systems and circumventing the limitation of the rising adsorbate concentration associated with Freundlich isotherm model. The model reduces to Freundlich isotherm at lower adsorbate concentrations while it predicts Langmuir model characteristics at higher adsorbate concentrations.

3.6. Adsorption kinetics studies

Pseudo-first-order, pseudo-second-order, and inter-particle diffusion models were applied to adsorption kinetics data (Table 5). Higher r^2 values for the entire concentration range and near $q_{e,exp}$ and $q_{e,cal}$ values confirm applicability of pseudo-second-order model (Table 6). To identify the diffusion mechanism, kinetics data were fitted to intra-particle diffusion model [33]. Fig. 6 represents Weber and Morris (q_t versus $t^{1/2}$) plot for the adsorption of BR2 on AI at various concentrations. For the entire BR2 concentration range, the plots were nonlinear over the entire range of contact time. This indicates that BR2 adsorption on AI was a multi-step process, involving adsorption on the external surface and diffusion into the interior pores of the AI. Thus, BR2 adsorption mechanism on AI involves migration of BR2 form the bulk of the solution to the AI surface, thereafter boundary layer diffusion and binding on active sites on AI surface. Finally, intra-particle diffusion occurs to the interior pores of AI. It should be pointed out here if intra-particle diffusion is the sole rate limiting step than (q_t vs. $t^{1/2}$) plot will pass through the origin [34] which was not a case in this study. It may be concluded that surface adsorption and intra-particle diffusion were concurrently operating during the adsorption of BR2 on AI. The intra-particle diffusion rate constant (K_i) increased with increase in BR2 concentration. The driving force of diffusion plays a critical role during adsorption process. The increase is BR2 concentration results in an increase in the driving force, which in turn increases BR2 diffusion rate. Intercept (I) of Weber and Morris plot gives an idea about the thickness of the boundary layer. Larger the I, greater the boundary layer effect. Data showed increase in I from 3.8 to 19.9 mg/g with increase in initial BR2 concentration from 25 to

Table 5
Kinetics models

Model	Equation	Parameters
Pseudo-first-order	$\log(q_e - q_t) = \log q_e - \frac{K_1}{2.303} \times t$	k_1(1/min), q_e (mg/g)
Pseudo-second-order	$\frac{t}{q_t} = \frac{1}{k_2 q_e^2} + \frac{1}{q_e} \times t$	k_2(mg/g min), q_e (mg/g)
Intra-particle diffusion	$q_t = k_i t^{1/2} + I$	k_i (mg/g $\text{min}^{1/2}$), I (mg/g)

Table 6
Kinetic parameters for BR2 adsorption on AI

C_o (mg/L)	$q_{e,exp}$ (mg/g)	Pseudo-first-order			Pseudo-second-order			Intra-particle diffusion		
		k_1 (1/min)	$q_{e,cal}$ (mg/g)	r^2	k_2 (g/mg min)	$q_{e,cal}$ (mg/g)	r^2	k_i (mg/g $\text{min}^{1/2}$)	I (mg/g)	r^2
25	9.55	0.0069	8.05	0.928	0.00002	9.77	0.999	0.143	3.83	0.626
50	26.94	0.0064	21.10	0.899	0.00049	27.03	0.997	0.361	11.25	0.590
75	39.60	0.0069	33.47	0.954	0.00032	39.84	0.997	0.548	15.80	0.610
100	51.87	0.0062	43.40	0.945	0.00023	52.91	0.999	0.757	19.66	0.663
125	62.92	0.0046	56.95	0.977	0.00013	64.10	0.996	0.955	19.67	0.737
150	72.77	0.0039	36.58	0.729	0.00956	75.19	0.999	1.201	19.90	0.808

150 mg/L revealing increase in concentrations promoting the effect on boundary layer diffusion.

3.7. Effect of background electrolyte

Wastewater streams along with dyes contain different anions and cations possibly posing hindrance during the adsorption process. Concerning the interfering effect of counter ions on adsorption in this study, we have checked their effect on adsorption. Sodium chloride (NaCl) at various concentrations (0.10–0.25 M) was taken as a background electrolyte. A decrease in BR2 (C_o—150 mg/L) adsorption from 64.5 to 58.2 mg/g was observed with increase in NaCl ionic strength from 0.10 to 0.25 M, respectively (Fig. 7). The observed decrease in BR2 adsorption on AI was 10% with 2.5-fold increase in NaCl concentration. This could be attributed to competitive effect between BR2 ions (cationic dye) and Na^+ ions to occupy available sites on adsorbent surface [35]. Slight increase in adsorbate dissociation and an enhanced aqueous solubility might also be the possible reason for decrease in adsorption. Our

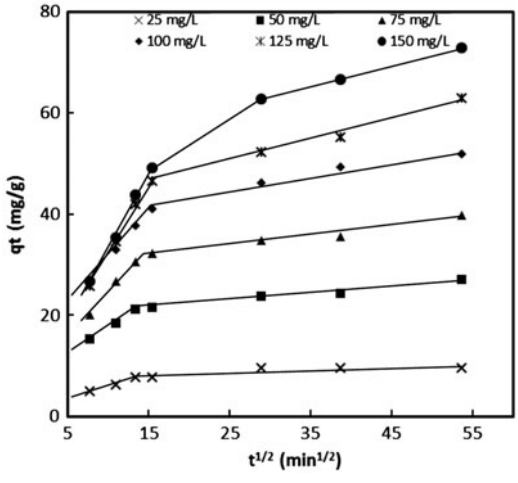

Fig. 6. Intra-particle diffusion model for BR2 adsorption on AI.

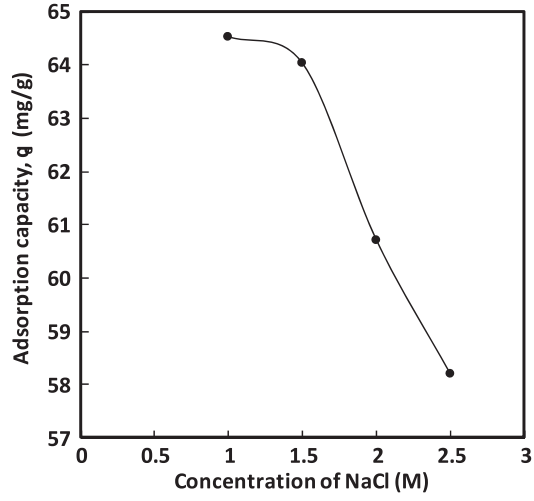

Fig. 7. Effect of electrolyte on BR2 adsorption on AI.

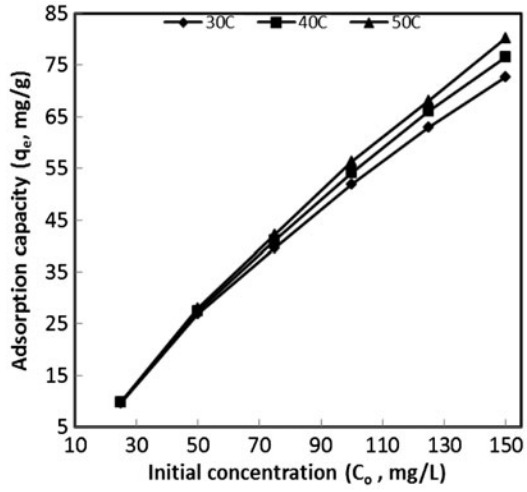

Fig. 8. Effect of temperature on BR2 adsorption on AI.

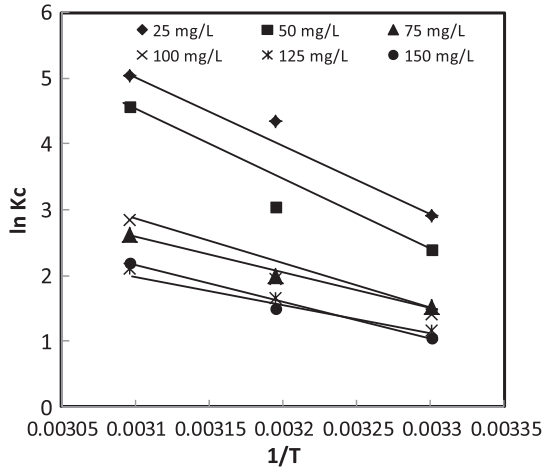

Fig. 9. Van't Hoff plots at various BR2 concentrations.

results were in good agreement with previously reported results for MB adsorption on sludge ash in presence of NaCl as ionic salt [36].

3.8. Effect of temperature

Thermodynamics studies were carried out at various initial BR2 concentrations (25–150 mg/L) by varying temperature from 30 to 50°C. The increase in adsorption capacity was observed with increase in adsorbate solution temperature confirming endothermic nature of adsorption process (Fig. 8). For studied concentration range, the adsorption capacity increased from 9.55 to 72.77 mg/L, 9.85 to 76.5 mg/L, and 9.90 to 80.31 mg/L at 30, 40, and 50°C, respectively. The effect of temperature on BR2 adsorption was appreciably visible at higher BR2 concentrations.

Various thermodynamics parameters such as standard free energy change (ΔG°), standard enthalpy change (ΔH°), and standard entropy change (ΔS°) were evaluated. Standard free energy change (ΔG°) can be calculated as:

$$\Delta G^\circ = -RT \ln K_c \tag{3}$$

where R (8.314 J/mol K) is a universal gas constant, T (K) is an absolute temperature, K_c is a constant.

$$K_c = \frac{C_{Ae}}{C_e} \tag{4}$$

where C_{Ae} and C_e are BR2 concentration on adsorbent and in solution at equilibrium, respectively.

Van't Hoff equation was used to determine ΔH° and ΔS° values. The equation is given as

$$\ln K_c = \frac{\Delta S^\circ}{R} - \frac{\Delta H^\circ}{RT} \tag{5}$$

By plotting $\ln K_c$ vs. $1/T$, the slope and I of the plot give thermodynamic parameters (Fig. 9). The experimental results obtained showed that the BR2 adsorption increases with an increase in temperature. The thermodynamic parameters were listed in Table 7. The adsorption at various BR2 concentrations was endothermic as indicated by positive values of ΔH°

Table 7
Thermodynamics parameters for BR2 adsorption on AI

Initial concentration (C_o, mg/L)	ΔH° (kJ/mol)	ΔS° (J/mol K)	ΔG° (kJ/mol)			r^2
			30°C	40°C	50°C	
25	84.87	305.61	−7.47	−11.32	−13.55	0.9693
50	84.83	299.36	−6.25	−8.06	−12.29	0.9430
75	39.18	143.32	−4.31	−5.51	−7.19	0.9916
100	51.80	183.92	−4.10	−5.40	−7.80	0.9720
125	32.34	118.59	−3.60	−4.77	−5.97	0.9997
150	38.69	138.50	−3.37	−4.43	−6.16	0.9831

and spontaneous as indicated by the negative value of ΔG°. Generally, for physisorption ΔG° should be in range −20–40 kJ/mol and for chemisorption ΔG° should be in range −400 to 80 kJ/mol [37]. During the present study, the ΔG° at various BR2 concentrations and reaction temperatures falls in range −13.55 to 3.37 kJ/mol indicating physisorption process agreeing with previously reported results for congo red adsorption on Ca-bentonite [38]. The positive value of ΔS° indicates randomness at solid/solution interface.

4. Conclusions

Batch scale studies were carried out to testify adsorption potential of AI for BR2. Acidic sites dominate over AI surface. Spectroscopic analysis showed active involvement of hydroxyl (–OH) and carboxyl (–COOH) functionalities in adsorption process. Optimum BR2 adsorption (15.6 mg/g) on AI was observed at pH: 7. Adsorption capacity increases from 9.54 to 72.74 mg/g with increase in BR2 concentration from 25 to 150 mg/g, respectively, with equilibration time varies between 840 and 1,500 min. Linear, nonlinear isotherms, and statistical error functions studies showed Sips model as a best applicable model to data. The maximum monolayer adsorption capacity (q_m) as obtained from linearized form of Langmuir model was 91.74 mg/g. Kinetics studies showed pseudo-second-order model applicability. Sodium chloride, a background electrolyte showed 10% decrease in adsorption capacity with 2.5-fold increase in BR2 concentration confirming no profound decrease in adsorption capacity. This shows effective utility of AI for BR2 removal even in presence of interfering ions. Thermodynamics studies showed endothermic and physical nature of adsorption process. Hence, we can conclude that the utility of AI for BR2 adsorption could be a better waste management alternative.

Acknowledgment

The authors wish to thank the Islamic Azad University, Omidiyeh Branch for their financial support and valuable assistance.

Nomenclature

γ	—	Redlich–Peterson model exponent
τ	—	Toth model exponent
n	—	Freundlich model exponent
λ	—	Sips model exponent
a_T	—	Toth saturation capacity (mg/g)
C_o	—	initial concentrations of dye solution (mg/L)
C_t	—	concentration of dye solution at time, t (mg/L)
C_e	—	concentration of dye solution at equilibrium (mg/L)
I	—	thickness of boundary layer (mg/g)
Ki	—	intra-particle diffusion constant (mg/g $\text{min}^{1/2}$)
k_1	—	pseudo-first-order rate constant (1/min)
k_2	—	pseudo-second-order rate constant (mg/g min)
k_F	—	Freundlich constant [(mg/g) $(\text{L/mg})^{1/n}$]
k_L	—	Langmuir constant (L/mg)
k_{RP}	—	Redlich–Peterson constant rate (L/g)
k_T	—	Toth constant (L/g)
k_S	—	Sips constant (L/g)
m	—	mass of adsorbent added to the solution (g)
N	—	number of observations
q_t	—	adsorption capacity at any time, t (mg/g)
q_e	—	adsorption capacity at equilibrium (mg/g)
q_m	—	maximum monolayer adsorption capacity (mg/g)
R_L	—	dimensionless constant
R	—	universal gas constant (8.314 J/mol K)
t	—	contact time (min)
T	—	temperature (°C)
V	—	volume of the dye solution (L)
ΔG°	—	standard free energy change (kJ/mol)
ΔH°	—	standard enthalpy change (kJ/mol)
ΔS°	—	standard entropy change (J/mol K)

References

[1] I. Eichlerova, L. Homolka, F.E. Nerud, Decolorization of high concentrations of synthetic dyes by the white rot fungus Bjerkandera adusta strain CCBAS 232, Dyes Pigm. 75 (2007) 38–44.
[2] S.C.R. Santos, V.J.P. Vilar, R.A.R. Boaventura, Waste metal hydroxide sludge as adsorbent for a reactive dye, J. Hazard. Mater. 153 (2008) 999–1008.
[3] S.B. David, Factors associated with textile pattern dermatitis caused by contact allergy to dyes, finishes, foams, and preservatives, Dermatol. Clin. 27 (2009) 309–322.
[4] Y.S. Al-Degs, M.I. El-Barghouthi, A.H. El-Sheikh, G.M. Walker, Effect of solution pH, ionic strength, and temperature on adsorption behavior of reactive dyes on activated carbon, Dyes Pigm. 77 (2008) 16–23.
[5] S. Hosseini, M.A. Khan, M.R. Malekbala, W. Cheah, T.S.Y. Choong, Carbon coated monolith, a mesoporous material for the removal of methyl orange from aqueous phase: Adsorption and desorption studies, Chem. Eng. J. 171 (2011) 1124–1131.
[6] A. Kuleyin, F. Aydin, Removal of reactive textiledyes (remazol brillant blue R and remazol yellow) by surfactant-modified natural zeolite, Environ. Prog. Sustainable Energy 30(2) (2011) 141–151.
[7] J.H. Huang, K.L. Huang, S.Q. Liu, A.T. Wang, C. Yan, Adsorption of rhodamine B and methyl orange on a hypercross-linked polymeric adsorbent in aqueous solution, Colloid Surf. A: Physicochem. Eng. Aspect. 330 (2008) 55–61.
[8] H. Chen, J. Zhao, G. Dai, Silkworm exuvia a new non-conventional and low-cost adsorbent for removal of methylene blue from aqueous solutions, J. Hazard. Mater. 186 (2010) 1320–1327.

[9] G. Crini, Non-conventional low-cost adsorbents for dye removal: A review, Biores. Technol. 97 (2006) 1061–1085.
[10] A. Mittal, D. Jhare, J. Mittal, Adsorption of hazardous dye eosin yellow from aqueous solution onto waste material de-oiled soya: Isotherm, kinetics and bulk removal, J. Mol. Liq. 179 (2013) 133–140.
[11] A. Mittal, V. Thakur, J. Mittal, H. Vardhan, Process development for the removal of hazardous anionic azo dye congo red from wastewater by using hen feather as potential adsorbent, Desalin. Water Treat. 179 (2013). doi: 10.1080/19443994.2013.785030.
[12] A. Mittal, V. Thakur, V. Gajbe, Adsorptive removal of toxic azo dye amido black 10B by hen feather, Environ. Sci. Pollut. Res. 20 (2013) 260–269.
[13] A. Mittal, V. Thakur, V. Gajbe, Evaluation of adsorption characteristics of an anionic azo dye brilliant yellow onto hen feathers in aqueous solution, Environ. Sci. Pollut. Res. 19 (2012) 2438–2447.
[14] A. Mittal, R. Jain, J. Mittal, S. Varshney, S. Sikarwar, Removal of yellow ME 7 GL from industrial effluent using electrochemical and adsorption techniques, Int. J. Environ. Pollut. 43(4) (2010) 308–323.
[15] A. Mittal, R. Jain, J. Mittal, M. Shrivastava, Adsorptive removal of hazardous dye quinoline yellow from waste water using coconut-husk as potential adsorbent, Fresenius Environ. Bull. 19(6) (2010) 1–9.
[16] A. Mittal, L. Kurup, Column operations for the removal & recovery of a hazardous dye 'acid red-27' from aqueous solutions, using waste materials—Bottom ash and de-oiled soya, Ecol. Environ. Conserv. 13(2) (2006) 181–186.
[17] A. Mittal, Removal of the dye, amaranth from waste water using hen feathers as potential adsorbent, Electron. J. Environ. Agric. Food Chem. 5(2) (2006) 1296–1305.
[18] H. Chen, P.L. Morrell, V.E.T.M. Ashworth, M. De La Cruz, M.T. Clegg, Tracing the geographic origins of major avocado cultivars, J. Hered. 100 (2008) 56–65.
[19] L.A. Rodrigues, M.L.C.P. da Silva, M.O. Alvarez-Mendes, A.D. Reis Coutinho, G.P. Thim, Phenol removal from aqueous solution by activated carbon produced from avocado kernel seeds, Chem. Eng. J. 174 (2011) 49–57.
[20] R. Devi, Innovative technology of COD and BOD reduction from coffee processing wastewater using avocado seed carbon (ASC), Water Air Soil Pollut. 207 (2010) 299–306.
[21] E. Cristiani-Urbina, A.R. Netzahuatl-Munoz, M.D.C. Cristiani-Urbina, Removal of hexavalent and total chromium from aqueous solution by avocado shell, Chem. Eng. Trans. 24 (2011) 1339–1344.
[22] D.H. Lataye, I. Mishra, I.D. Mall, Removal of pyridine from aqueous solution by adsorption on bagasse fly ash, Ind. Eng. Chem. Res. 45 (2006) 3934–3943.
[23] T.N. McCaig, Extending the use of visible/near-infrared reflectance spectrophotometers to measure color of food and agricultural products, Food Res. Int. 35 (2002) 731–736.
[24] K.V. Kumar, Pseudo-second order models for the adsorption of safranin onto activated carbon: Comparison of linear and non-linear regression methods, J. Hazard. Mater. 142(1–2) (2007) 564–567.
[25] R.W. Sabnis, Handbook of Biological Dyes and Stains, Synt. Ind. Appl., John Wiley and Sons, Hoboken, NJ, 2010.
[26] G. Vijayakumar, C.K. Yoo, K.G.P. Elango, M. Dharmendirakumar, Adsorption characteristics of rhodamine B from aqueous solution onto baryte, Clean—Soil Air Water. 38 (2) (2010) 202–209.
[27] M.A. Khan, M. Ngabura, T.S.Y. Choong, H. Masood, L.A. Chuah, Biosorption and desorption of Nickel on oil cake: Batch and column studies, Bioresour. Technol. 103 (2012) 35–42.
[28] F. Doulati Ardejani, K. Badii, N.Y. Limaee, S.Z. Shafaei, A.R. Mirhabibi, Adsorption of direct Red 80 dye from aqueous solution onto almond shells: Effect of pH, initial concentration and shell type, J. Hazard. Mater. 151 (2008) 730–737.
[29] F. Gode, E. Pehlivan, Removal of chromium(III) from aqueous solutions using Lewatit S 100: The effect of pH, time, metal concentration and temperature, J. Hazard. Mater. 136 (2006) 330–337.
[30] A. Atelekli, F. Geyik, Artificial neural networks (ANN) approach for modeling of removal of Lanaset Red G on *Chara contraria*, Biores. Technol. 102 (2011) 5634–5638.
[31] F.D.R. Gimbert, N. Morin-Crini, F.O. Renault, P.M. Badot, G. Crini, Adsorption isotherm models for dye removal by cationized starch-based material in a single component system: Error analysis, J. Hazard. Mater. 157 (2008) 34–46.
[32] S.J. Allen, Q. Gan, R. Matthews, P.A. Johnson, Comparison of optimised isotherm models for basic dye adsorption by kudzu, Biores. Technol. 88 (2003) 143–152.
[33] J. Chen, H. Yang, Z. Ring, Study of intra-particle diffusion effect on hydrodesulphurization of dibenzothiophenic compounds, Catal. Today 109 (2005) 93–98.
[34] Y.S. Ho, Removal of copper ions from aqueous solution by tree fern, Water Res. 37 (2003) 2323–2330.
[35] R. Han, W. Zou, W. Yu, S. Cheng, Y. Wang, J. Shi, Biosorption of methylene blue from aqueous solution by fallen phoenix tree's leaves, J. Hazard. Mater. 141 (2007) 156–162.
[36] C.-H. Weng, Y.-F. Pan, Adsorption characteristics of methylene blue from aqueous solution by sludge ash, Colloids Surf. A: Physicochem. Eng. Aspect. 274 (2006) 154–162.
[37] E. Eren, B. Afsin, Investigation of a basic dye adsorption from aqueous solution onto raw and pre-treated bentonite surfaces, Dyes Pigm. 73 (2007) 162–167.
[38] L. Lian, L. Guo, C. Guo, Adsorption of congo red from aqueous solutions onto Ca bentonite, J. Hazard. Mater. 161 (2009) 126–131.